THE JOURNAL OF PHYSICAL CHEMISTRY LETTERS
A JOURNAL OF THE AMERICAN CHEMICAL SOCIETY

pubs.acs.org/JPCL Letter

Mechanism of Ag^+-Induced Folding of a Bacterial Peptide from Replica-Exchange Molecular Simulations

Florian E. C. Blanc,* Maggy Hologne, Marion Girod, Mélodie Demontrond, Henry Chermette, and Olivier Walker*

Cite This: https://doi.org/10.1021/acs.jpclett.6c00044 Read Online

ACCESS | Metrics & More | Article Recommendations | Supporting Information

ABSTRACT: Interactions between proteins and metal cations are central to biochemical processes and shape protein structures. SilE, an intrinsically disordered protein involved in bacterial silver resistance, folds into α-helices upon binding Ag^+ ions. Focusing on the B1 peptide fragment from SilE, we investigate the mechanism of Ag^+-induced folding with atomistic simulations and experiments. Guided by Mass Spectrometry and NMR, we prepare a structural model of Ag^+-bound B1, which we parametrize using DFT. Then, with replica-exchange simulations and deep learning, we map B1's folding landscape and how it is shaped by Ag^+. Specifically, Ag^+ binding promotes folding by lowering the entropy of the disordered state and stabilizing the folded state. We also describe how Ag^+ alters the folding pathways. Overall, we improve our understanding of metal-induced protein folding and lay the groundwork for further computational investigations of the bacterial silver-resistance machinery.

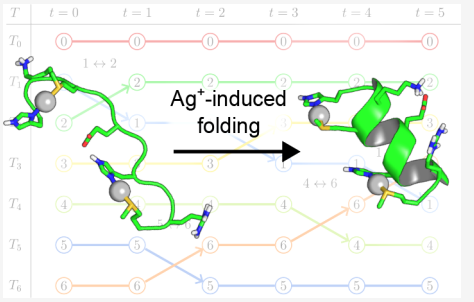

Interaction with metal cations can shape the conformational landscapes of proteins in several ways. Metals can promote protein unfolding,[1] misfolding or aggregation, which may lead to neurodegenerative disorders.[2,3] Conversely, metals at an optimum concentration are essential for proteins, and ≈33% of protein structures in the PDB have at least one metal ion (https://www.rcsb.org/). Metals can be involved in folding[4,5] and help maintain the 3D structure of proteins.[6] For example, recent research by our group[7−9] and others[10] has showed that the bacterial intrinsically disordered protein SilE locally folds into α-helices upon binding silver cations Ag^+. The present paper is concerned with understanding the mechanism and energetics of this Ag^+-induced folding through Molecular Dynamics (MD) simulations and experiments.

SilE (Figure 1A) is an essential member of the *sil* silver-efflux machinery, which confers Gram-negative Bacteria resistance against silver toxicity.[11−13] The antimicrobial properties of silver have been used since Antiquity.[14] Novel silver-based antibacterials could help counter rising antibioresistance,[15,16] but for this it is critical to address bacterial resistance to silver.[17] Understanding the molecular underpinnings of the silver-resistance machinery would facilitate this endeavor by guiding drug discovery efforts.

SilE is natively disordered but folds locally into α-helical segments upon binding Ag^+ cations.[9] This feature is retained by peptide fragments encompassing the silver binding sites composed of HXXM or MXXH motifs.[7,8,18,19] The ability of SilE to bind free Ag^+ is crucial for the *sil* machinery, which makes SilE an attractive—albeit challenging—pharmacological target. However, the functional importance of its folding upon binding of Ag^+ is not well understood. For instance, it is

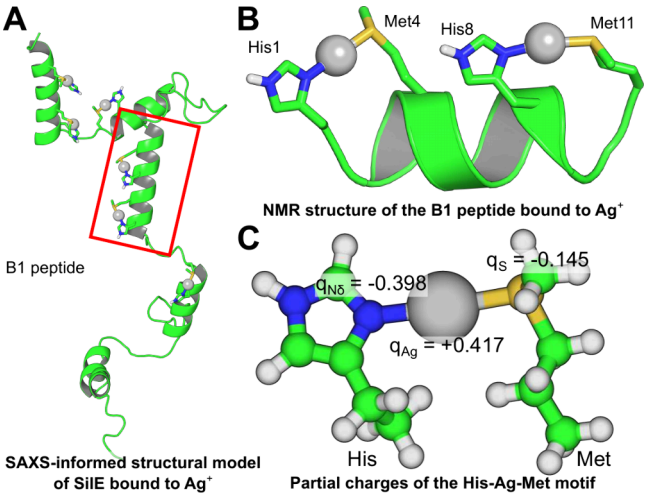

Figure 1. Description of the B1 peptide and the bonded model for His−Ag^+−Met. A. Representative structure of Ag^+-bound full-length SilE from SAXS measurements[9] showing the folded α-helical silver-binding regions. B. NMR structure of the Ag^+-bound B1 peptide.[8] For clarity, only polar hydrogens are shown. C. Bonded model with C-RESP2 partial charges for His-Nδ, Ag and Met-S derived from DFT calculations. The full list of partial charges is given in Table S2.

Received: January 7, 2026
Revised: January 30, 2026
Accepted: February 2, 2026

unclear whether the helical motifs modulate the affinity of SilE for Ag^+ or enable functional interactions with other *sil* proteins.[20,21] More generally, how silver cations could stabilize helical structures in peptides and proteins has been poorly described.

Addressing this question with atomically detailed simulations of Ag^+-induced folding is challenging for two reasons. First, MD simulations of peptide folding require extensive sampling and a force field that can describe the unfolded state accurately.[22,23] Second, classical force fields struggle to describe d-group metallic cations and their interactions with proteins.[24] Polarizable force fields and Quantum Mechanics/Molecular Mechanics (QM/MM) can accurately describe metal centers in proteins while enabling some conformational sampling,[25−27] but their computational cost makes their use for folding simulations challenging.[28] Despite their limitations, fixed-charge force fields have shown successes in metal modeling,[24] for example, when *ad hoc* modifications are incorporated to approximate the effects of polarization.[29−31] Parametrization of transition metal cations for fixed-charge or polarizable force fields remains an active topic of research. Lennard-Jones parameters for nonbonded cations including Ag^+ have been developed by Merz et al.[32,33] Their most recent parameter set describes His-Ag^+ interactions well[34−36] but requires a nonstandard "12-6-4" interaction potential[37,38] that precludes widespread adoption. Very recently, Manciocchi et al. reported on a standard ("12-6") Ag^+ model[39] calibrated to reproduce binding affinities to SilE tetrapeptide fragments.[7] This model is promising, but it remains unclear whether it can capture how interactions with Ag^+ affect protein conformations, as discussed below. Alternatively, bonded models that treat the interaction with Ag^+ as effectively covalent have been proposed. Chen et al. developed a bonded model for the interaction with cytosine,[40] and Lithgo et al. for the interaction with the SilF protein.[27] In both studies, parameters were developed for the AMBER force fields; we are not aware of similar efforts for the CHARMM force fields. In addition, to our knowledge, no previous work has specifically investigated the structural consequences of binding of Ag^+ to proteins with an atomistic level of details.

Here, we lay the groundwork toward atomistic simulations of full-length SilE Ag^+-induced folding by focusing on an 11-residue peptide fragment from SilE,[8] called B1 (HQKMVESHQRM), which contains two HXXM silver-binding motifs. First, we collect experimental evidence from mass spectrometry (MS) and nuclear magnetic resonance (NMR) in favor of a "binding then folding" mechanism. This motivates simulating the folding of B1 with a bonded Ag^+ model. We then develop a CHARMM-compatible bonded model for the His−Ag^+−Met coordination complex using electronic structure calculations. In so doing, we address the gap of the Ag^+-protein bonded model for the CHARMM force-field family. Next, we explore the conformational space of B1 in the presence and absence of Ag^+ using temperature-replica-exchange molecule dynamics (T-REMD) simulations in explicit solvent (200 μs of aggregate MD sampling). Analysis of the simulations by rigorous free-energy reweighting and deep learning maps the conformational landscape of B1 and shows that our model correctly captures the Ag^+-induced α-helix stabilization. We evaluate the effect of alternative parametrizations of our bonded model on the folding equilibrium. We introduce a postprocessing procedure based on the string method[41] to reveal the mechanistic pathways of B1 folding and how they change when Ag^+ is bound. Overall, our study provides a comprehensive picture of B1's Ag^+-induced folding.

Previous NMR experiments have shown that B1's folding and binding to Ag^+ are coupled[8] but did not address whether this coupling proceeds through a conformational selection mechanism (Ag^+ binds preferentially to minority folded conformers, shifting the equilibrium toward the folded state) or whether Ag^+ binds to disordered conformers and directly induces folding. We first set out to answer this question experimentally. MS shows unambiguously that the major form of B1 under saturating Ag^+ conditions is bound to two Ag^+ ions (Figure 2A). Since MS samples were prepared in strongly

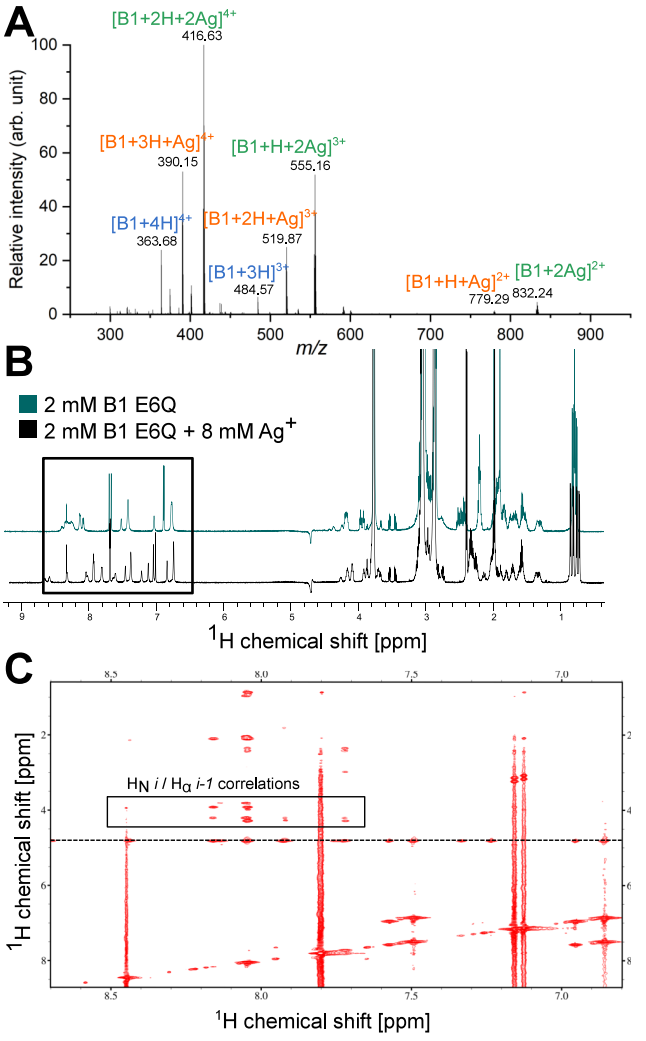

Figure 2. Experimental data on B1. A. MS spectrum of B1+Ag^+, with the main peak corresponding to B1 + 2Ag^+. B. 1D ^{1}H NMR spectra of B1 E6Q with and without Ag^+ recorded at a ^{1}H frequency of 700 MHz and 293 K. The rectangle indicates the amide and aromatic protons region. C. 2D ^{1}H−^{1}H NOESY spectrum of B1 E6Q in the presence of Ag^+.

denaturating conditions (≈12 M methanol, Supplementary Text 6), this demonstrates that Ag^+ binding by B1 does not require prefolding into an α-helix. NMR characterization of a B1 E6Q mutant provides additional information (Supplementary Text 5). Similar to wild-type B1,[8] the 1D ^{1}H NMR spectrum of B1 E6Q indicates that this mutant is disordered in the free form (Figure 2B). In the presence of Ag^+, the ^{1}H

https://doi.org/10.1021/acs.jpclett.6c00044
J. Phys. Chem. Lett. XXXX, XXX, XXX−XXX

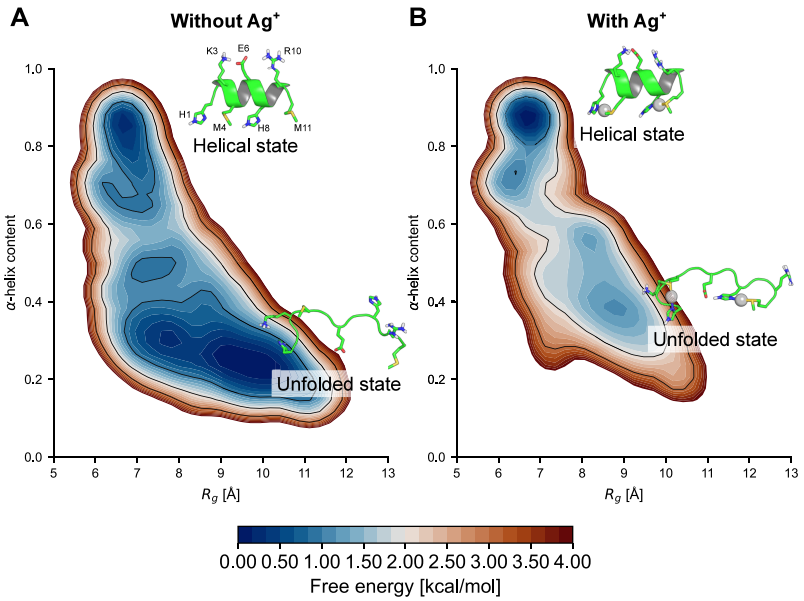

Figure 3. Free energy profiles along (R_g, α) reveal how Ag^+-binding shapes the folding landscape of B1. A. Simulation Free B1 (1). B. Simulation B1+Ag^+ C-RESP2 (1). Representative frames are shown; for clarity, only polar hydrogens are shown.

chemical shifts are perturbed (Figure 2B), indicating that B1 E6Q retains the capacity to bind Ag^+. Yet, unlike wild-type B1, the 2D NOESY spectrum of B1 E6Q in the presence of Ag^+ shows only sequential i, i + 1 correlations, indicating a disordered state (Figure 2C). Thus, B1 E6Q is able to bind Ag^+ but is unable to fold. Therefore, folding is not required for Ag^+ binding; instead, Ag^+ binding precedes and promotes folding in wild-type B1. This justifies developing and using a bonded model to investigate this process with MD simulations.

We thus developed a bonded model of His−Ag^+−Met in a linear geometry (Figure 1C), calibrated on Density Functional Theory (DFT) calculations and compatible with the CHARMM force fields (Supplementary Text 1). We used the Seminario method to determine force constants from the Hessian matrix computed at the DFT-optimized geometry;[42,43] see Table S1. Deriving CHARMM-compatible partial charges for systems containing transition metals, such as silver, is nontrivial because the standard parametrization approach relies on HF/6-31G* calculations, which are likely to describe such systems less accurately than correlated methods such as DFT. To address this challenge, we used an appropriate level of theory (PBE0/def2-TZVP),[44−47] and we introduced two key modifications to the RESP procedure.[48] First, we constrained partial charges of most atoms to their CHARMM standard values during the RESP calculation[49] (Table S2, Figure S1), a procedure we term C-RESP (for CHARMM-RESP). Second, we approximately accounted for solvent polarization using the RESP2 procedure by Gilson et al.[50] Motivations for these parametrization decisions are provided in Supplementary Text 1. Together, they yielded the C-RESP2 procedure for partial charge derivation.

We prepared 8 simulation systems that differed in three aspects: (i) presence or absence of Ag^+, (ii) whether the B1 peptide was wild-type or the B1E6Q mutant, and (iii) the parametrization scheme used for the His−Ag^+−Met motif; see Table S3. The observation that B1 folds into an α-helix when bound to Ag^+[8] points to a binding pattern in which the first Ag^+ cross-links the side chains of His1 and Met4, and the second Ag^+ cross-links His8 and Met11 (Figure 1B). All B1+Ag^+ simulations were prepared with this binding pattern. The alternative binding mode in which Ag^+ ions cross-link His1 to Met11, and His8 to Met4, would not be compatible with an α-helix. Instead, it may stabilize a β-hairpin configuration, which is not observed by NMR. We energy-minimized and equilibrated each model in a cubic box filled with CHARMM TIP3P water molecules[51] and 150 mM of Na^+ + Cl^-. From each equilibrated system, we ran T-REMD simulations,[52,53] with 64 replicas and temperatures ranging from 293 to 470 K chosen to balance extensive conformational sampling with efficient exchange;[54] see Supplementary Text 2 for the simulation parameters. Our replica-exchange simulations aggregate 200 μs of sampling (Table S3). For Ag^+-free B1 and B1+Ag^+ with the C-RESP2 parametrization, we ran two independent T-REMD simulations to assess the robustness of our findings. In all T-REMD simulations, the ≈20% observed exchange acceptance rate, reversible diffusion of replicas over temperature space (Figure S2), and overlapping potential energy distributions (Figure S3) suggest that the simulations have correctly explored the conformational space.

To get a global view of how Ag^+ binding affects the energetics of B1 folding, we evaluated the two-dimensional free energy landscapes at 293 K (i.e., the temperature of the NMR measurements[8]) along the radius of gyration R_g and the α-helix content[55] α of B1; see Figure 3 and Figure S4. α = 1.0 for a perfect α-helix and 0 for a fully disordered configuration. We used Multistate State Bennett Acceptance Ratio (MBAR) reweighting to combine the data collected at all temperatures, making optimal use of our simulations.[56] We then evaluated free energy landscapes by weighted Gaussian kernel density estimation (KDE), using the MBAR weights as implemented in *pymbar*[57] (see Table S4 for KDE bandwidths). The free energy landscapes show how Ag^+-binding shapes the folding landscape of the B1 peptide.

Both in the presence and in the absence of Ag^+, the free energy landscape exhibits two main local minima: the folded state encompasses compact (R_g ≈ 6.5 Å), α-helical configurations (α ≈ 0.9) ,and the unfolded state comprises a range of conformers with low α-helical content (α < 0.4).

https://doi.org/10.1021/acs.jpclett.6c00044
J. Phys. Chem. Lett. XXXX, XXX, XXX−XXX

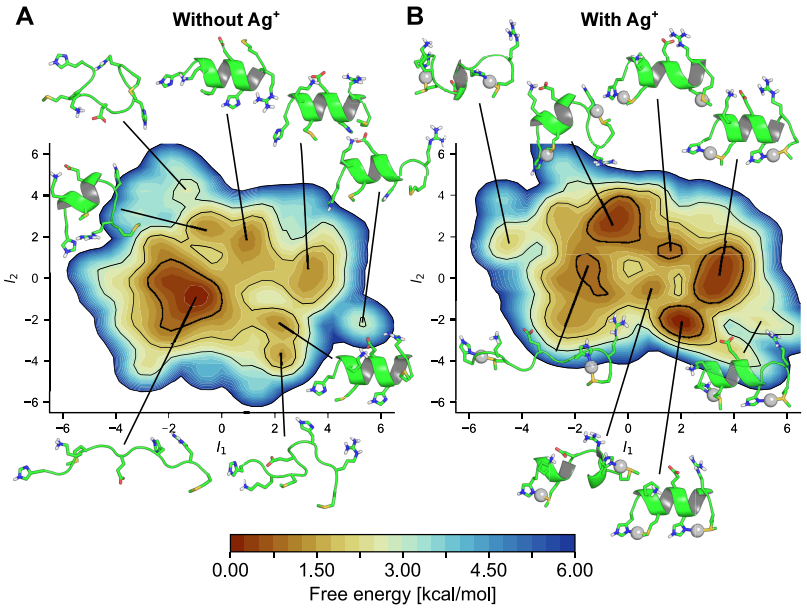

Figure 4. Free energy landscapes of B1 in the absence (A) and the presence (B) of Ag^+ along Isomap-transformed latent variables from the deep autoencoder reveal conformational substates. A. Simulation Free B1 (1). B. Simulation B1+Ag^+ C-RESP2 (1). Note that the free energy levels go up to 6 kcal mol^{-1}. For each metastable state, a representative simulation frame is shown; for clarity, only polar hydrogens are shown.

Thus, our T-REMD simulations successfully capture the folding of B1. In addition, we observed a marked effect of Ag^+ on the folding landscape. Whereas the simulations predict a preference for the unfolded state in the absence of Ag^+, Ag^+-binding stabilizes the folded state by ≈1.5 kcal mol^{-1} relative to the unfolded state. These trends are observed in two independent T-REMD simulations, both in the absence (simulations Free B1 (1) and (2)) and in the presence (simulations B1+Ag^+ C-RESP2 (1) and (2)) of Ag^+. This suggests that our bonded model of the His−Ag^+−Met motif reproduces the experimentally observed preference of B1 for an α-helical conformation when bound to Ag^+.[8] We assessed the parametrization sensitivity of the folding equilibrium by performing T-REMD simulations of models with partial charges derived through alternative procedures (Supplementary Text 1). With default C36m partial charges (with +1 charge on Ag), the predicted ground state is disordered rather than folded (Figure S6A). This suggests that accounting for the rearranged electronic density upon Ag^+ binding is important to capture the stabilization of the helical state. A model with C-RESP partial charges stabilizes the folded state slightly less than C-RESP2 charges, suggesting that accounting for polarization in water may add a small but important contribution (Figure S6B). Surprisingly, C-RESP or C-RESP2 charges averaged over conformational fluctuations (Supplementary Text 1) predict a disordered ground state (Figure S6C,D). Although the physical basis for this effect is currently unclear, these findings empirically support our C-RESP2 parametrization methodology as the one that best reproduces the experimentally observed conformational equilibrium.

Bound Ag^+ ions stabilize the folded state in two ways. First, the positively charged His−Ag^+−Met motifs are positioned opposite K3 and R10; this charge pattern may make the helix rigid through electrostatic repulsion. Second, bound Ag^+ ions promote the formation of helical turns H1:V5 and S7:M11 by restricting the conformational freedom of the peptide backbone. This is apparent from the reduced range of R_g values sampled in the unfolded state when Ag^+ is present (Figure 3), indicating that Ag^+ destabilizes both very compact and very extended conformers. This reduces the conformational entropy of the unfolded state, shifting the equilibrium toward the helical configuration in the presence of Ag^+.

In the folded state, residues K3 and R10 can both form salt bridges with residue E6; these salt bridges are collinear to the helical axis, which could stabilize the α-helix (Figure 3A,B) independently of whether Ag^+ is present. This observation explains why the B1 E6Q mutant does not fold into an α-helix when bound to Ag^+. T-REMD simulations of B1 E6Q show that, without Ag^+, the disordered state is favored even more than in the wild-type, in agreement with NMR (Figure S5). With bound Ag^+, the predicted ground state is helical, which may be inconsistent with NMR; however, the conformational preference for the helix is decreased relative to wild-type B1+Ag^+, suggesting that our model captures the trend. These findings support that E6 stabilizes the helical conformation through salt bridges with K3 and R10. Thus, in addition to H:M cross-linking by Ag^+, a centrally positioned, negative side chain also promotes helical folding.

To get a finer view of the conformational landscape of B1 than that afforded by R_g and α, we turned to machine learning. We trained an autoencoder (AE) neural network to reduce the dimensionality of the conformational space to 6. The AE takes as input a vector of atomic coordinates, projects it onto a 6-dimensional latent space, and then attempts to reconstruct the input from the projection. In so doing, the AE discovers 6 latent variables that describe the conformational landscape. Inspired by previous work,[58−60] we used a loss function combining the reconstruction error, a term enforcing decorrelation of the latent variables, and a "sketch-map" term that helps latent variables distinguish between conformational basins on medium distance scale, i.e., the most likely relevant substates.[61] We trained the AE on ≈20 million T-REMD simulation frames. Details on the AE architecture, training, and loss function are provided in Supplementary Text 3 and Figure S7. To visualize the 6-dimensional latent space, we reduced it

https://doi.org/10.1021/acs.jpclett.6c00044
J. Phys. Chem. Lett. XXXX, XXX, XXX−XXX

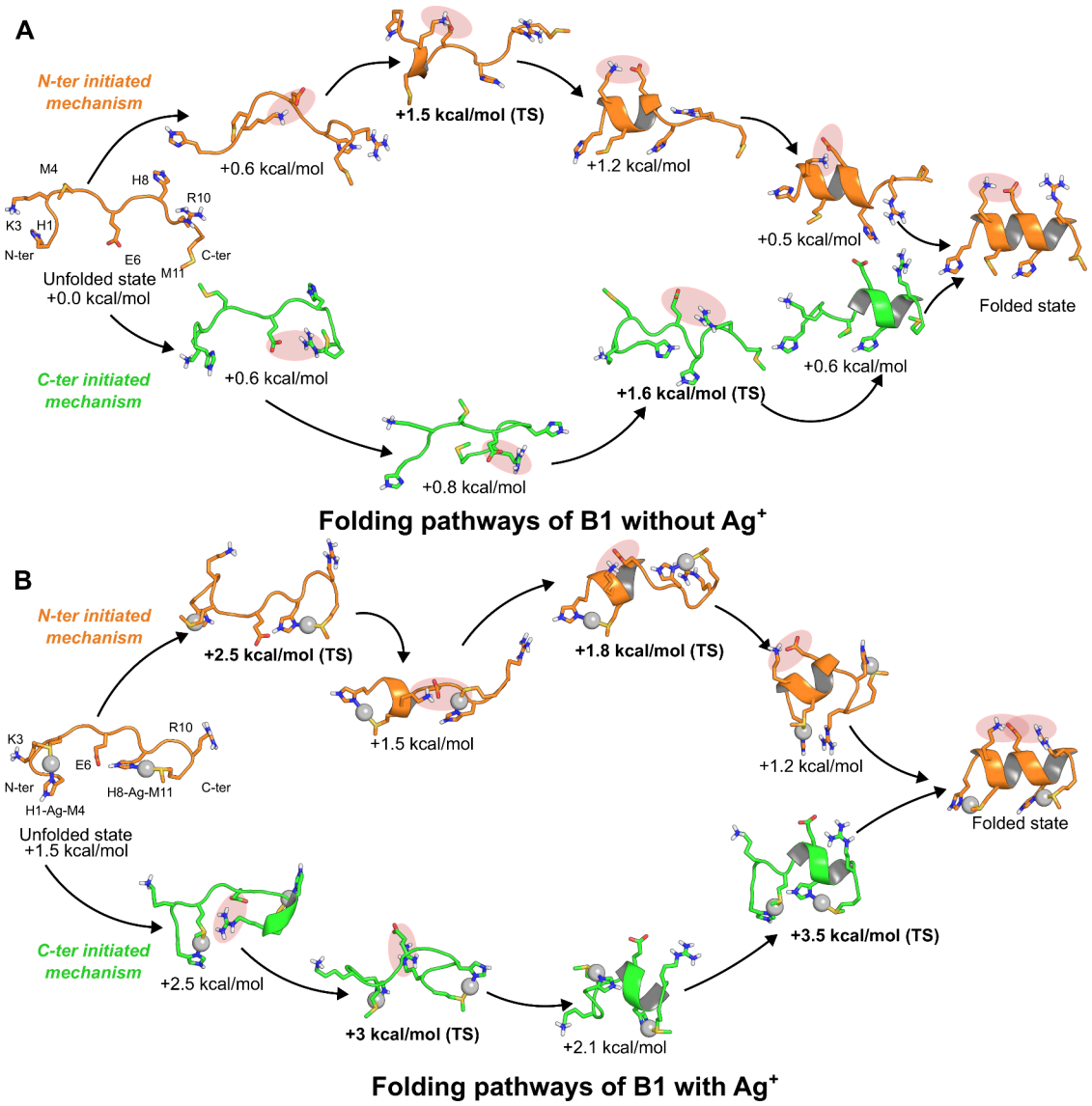

Figure 5. Folding pathways of B1 with and without Ag^+ from *post hoc* string method analysis of the replica-exchange simulations. A. Folding pathways in the absence of Ag^+, Simulation Free B1 (1). B. Folding pathways in the presence of Ag^+, Simulation B1+Ag^+ C-RESP2 (1). Orange: N-ter-initiated folding mechanism. Green: C-ter-initiated folding mechanism. TS: Transition State. The red shaded ellipse materializes the K3-E6 and E6-R10 salt bridges. Free energy levels are evaluated with respect to the folded state, and correspond to the free energy profiles of Figures S11A and S15A. For clarity, only polar hydrogens are shown.

to 2 dimensions with Isomap,[62,63] yielding variables l_1 and l_2. Next, we evaluated the free energy landscapes along l_1 and l_2 in the presence and absence of Ag^+ (Figure 4). This analysis reveals several metastable conformational states that are defined by their degree of folding. For example, the completely disordered state is found at ($l_1 \approx -1$, $l_2 \approx -1$), and the completely folded state encompasses two basins ($l_1 \approx 2$, $l_2 \approx -2$) and ($l_1 \approx 3$, $l_2 \approx 0$). Partially folded conformers are also identified, e.g., at ($l_1 \approx -0.5$, $l_2 \approx 2.5$) where the N-terminal half is folded, whereas the C-terminal half is disordered. Most of these states are present in both the apo and Ag^+-bound B1 peptide, and Ag^+-binding shifts the population toward partially or fully folded conformations.

The AE thus yields a detailed picture of the folding landscape of B1 and its modulation by Ag^+. However, it is not designed to identify folding pathways. We therefore developed a *post hoc* variant of the string method in collective variables (CVSM)[41,64−66] to extract Minimum Free Energy Paths (MFEPs) from our T-REMD simulations (described in Supplementary Text 4). We used it to compute folding MFEPs in a subspace defined by 6 collective variables describing the folding process (Table S6). These Human-designed CVs reflect the secondary structure content of B1, its global shape, and the formation of K3-E6 and E6-R10 salt bridges. Interestingly, we find that they are well correlated with the AE-learnt descriptors l_1 and l_2 (Figures S8 and S9). From the string method analysis, we infer detailed sequences of events for α-helical folding of B1, compare competing pathways, and assess how the mechanism changes when Ag^+ is present.

Because the string method is sensitive to the guess path,[67] we considered two hypotheses for the folding pathway: N-ter-initiated folding (in which helical turns first form in N-terminal and propagate toward C-terminal), or conversely C-ter-initiated folding. In both the presence and the absence of Ag^+, we prepared a guess path in CV-space corresponding to

https://doi.org/10.1021/acs.jpclett.6c00044
J. Phys. Chem. Lett. XXXX, XXX, XXX−XXX

each hypothesis, independently relaxed these paths with our string method, and compared their highest free energy barriers to evaluate their contribution to the total folding flux. The results suggest that Ag^+-binding may amplify a pre-existing preference for N-ter-initiated folding (Figure 5, Figures S11, S13, S15, and S17).

In the absence of Ag^+ (Simulation Free B1 (1)), N-ter-initiated folding starts with the formation of the K3-E6 salt bridge, which remains stably formed throughout the transition. This promotes the formation of N-terminal helical turns H1:V5 and Q2:E6. Then, the remainder of the peptide progressively folds from N-ter to C-ter (Figure 5 A). Conversely, late formation of the E6-R10 salt bridge does not seem required for folding from N-ter, although configurations in which it is formed are seen. The transition state (+1.5 kcal mol^{-1} higher in free energy than the disordered configuration) exhibits formed K3-E6 salt bridges and a H1:V5 helix turn, and a partially formed Q2:E6 helix turn, suggesting that the formation of this turn is rate-limiting for N-ter initiated folding in the absence of Ag^+ ions. C-ter-initiated folding starts with the formation of the E6-R10 salt bridge, favoring the formation of a bent intermediate from which the backbone H-bond E6:R10 forms, followed by the backbone H-bonds V5:Q9, M4:H8, and S7:M11. The transition state (+1.6 kcal mol^{-1} higher in free energy than the disordered configuration) immediately precedes the formation of the first helical turn. The E6-R10 salt bridge, although important for the early stages of C-ter-initiated folding, does not persist throughout the transition and is generally less stable than the K3-E6 one. Thus, although they exhibit similar energetics (and therefore rates), N-ter- and C-ter-initiated folding proceed through qualitatively different pathways. The independent Free B1 (2) simulation yields essentially the same picture except that the K3-E6 salt bridge forms halfway through N-ter-initiated folding. This suggests that the formation of this salt bridge is not strictly required to initiate folding from the N-ter. Additionally, the barrier for C-ter-initiated folding is higher (2.2 kcal mol^{-1}) whereas the barrier for N-ter-initiated folding is virtually unchanged (1.6 kcal mol^{-1}). This may reflect a slight intrinsic preference for N-ter-initiated folding.

In the presence of Ag^+ (Simulation B1+Ag^+ C-RESP2 (1)), the preference for N-ter-initiated folding is more marked. The highest transition state for N-ter-initiated folding lies +2.5 kcal mol^{-1} higher in free energy than the folded state, versus +3.5 kcal mol^{-1} for C-ter-initiated folding. This 1 kcal mol^{-1} difference translates into N-ter-initiated folding accounting for a predicted ≈85% of the folding flux at 293 K. The independent B1+Ag^+ C-RESP2 (2) simulation predicts a smaller, 0.7 kcal mol^{-1} difference between the free energy barriers, but still favoring N-ter folding over C-ter, suggesting Ag^+ amplifies the pre-existing bias. Overall, our results suggest that Ag^+-induced folding of B1 is determined by partial prestructuration of the N-terminal and proceeds directionally from N-ter to C-ter. Interestingly, the first step of the mechanism entails the formation of an intermediate in which E6 interacts electrostatically with K3 and Ag^+ bound to H8:M11, revealing that Ag^+ changes the sequence of structural states along the folding pathway.

Using enhanced sampling simulations in explicit solvent with a bespoke bonded model, we describe in atomistic detail how binding of Ag^+ to His-Met motifs promotes α-helical folding of a bacterial peptide fragment. We evaluate the relative thermodynamic stability of the folded state with respect to the disordered state in the absence and presence of Ag^+. We deploy a self-supervised neural network to map the conformational landscape and assess how it is modulated by Ag^+. We find that Ag^+ binding shifts the balance in favor of the helical state by several effects. First, it creates a favorable charge repartition that provides electrostatic stabilization. Second, it preorganizes a helix nucleation site in N-ter by keeping the peptide groups of H1 and V5 in close proximity. Last, the His−Ag^+−Met cross-link restricts the accessible conformational space in the unfolded state, creating an entropic penalty in comparison to the free peptide. These effects are reminiscent of how human-designed stapled peptides promote α-helical folding.[68] SilE peptides like B1 represent a unique case of naturally occurring metal-controlled stapling, and could inspire novel switchable metal-cross-linked peptides,[69,70] a purpose for which Ag^+ has seldom been used.[71] In fact, our study illustrates how simulations can rationalize and even predict how metals induce α-helices to help design peptide-based supramolecular architectures.[72]

Our results suggest that Ag^+ binding amplifies a pre-existing preference for N→C helical propagation in the peptide's folding mechanism. This is consistent with earlier computational and experimental evidence for N→C helical propagation in the folding of α-helical peptides.[73,74] In fact, the laser-induced temperature-jump infrared spectroscopy technique used by Acharrya et al.[74] could be directly applied to validate our proposed folding mechanism for the B1 peptide. In addition, we note that our string method analysis, although effective to infer dominant folding pathways, cannot account for off-pathway states —kinetic traps— that would slow down folding.[75] Determining how these may influence folding kinetics would require complementary analyses with, e.g., Markov State Models.[74]

We used a bonded model in which Ag^+ binding to His and Met is effectively covalent and irreversible, which assumes that Ag^+ binding precedes helix folding and cannot capture alternative scenarios in which helix prefolding is required for binding.[4] This choice is supported by our simulations of the free B1 peptide, which show only marginal helix formation in the absence of Ag^+, by our MS and NMR measurements indicating Ag^+ binding without helix formation, and by the ability of HXXM tetrapeptides—too short to form helices—to bind Ag^+.[7,19]

By construction, the bonded model enables enhanced sampling of the bound state without "contamination" from unbound configurations, which helps isolate the reduction of conformational entropy brought about by Ag^+ binding. Although this may bias the folding mechanism, our experimental evidence for folding after binding suggests that the resulting pathways remain physically representative. In this sense, simulations with a bonded model provide a clearer separation between binding and folding than that accessible to MS and NMR, highlighting the complementarity of these approaches.

Because of the lack of an adequate method for transition metal parametrization in CHARMM force fields, we adopted a nonstandard scheme for partial charge derivation. This scheme, termed C-RESP2, seeks to recover missing polarization effects through linear combination of vacuum and aqueous RESP charges, following the approach of Gilson et al.[50] Empirical comparison with alternative parametrizations indicates that C-RESP2 best reproduces the experimental folding equilibrium,

https://doi.org/10.1021/acs.jpclett.6c00044
J. Phys. Chem. Lett. XXXX, XXX, XXX−XXX

making it suitable for the present mechanistic analysis. Whether this approach can be readily generalized to other transition-metal−containing systems remains an open question.

More broadly, our results support the use of bonded models to investigate protein-metal interactions. Lithgo and coworkers recently reported on a joint experimental and computational study of SilF,[27] another Sil protein.[21] These authors parametrized Ag^+ binding to SilF as a bonded model for the AMBER force fields, which they find agrees with QM/MM simulations. Our parametrization follows similar lines but is tailored for CHARMM force fields instead. Thus, both our work and that of Lithgo et al.[27] suggest that bonded models for Ag^+ binding to proteins can enable functional insight. Moreover, we note that SilF is a structured protein for which no major rearrangement occurs upon Ag^+ binding, unlike that of the B1 peptide studied here. At the same time, Manciocchi et al. developed a nonbonded model of the Ag^+ cation optimized to reproduce the thermodynamics of interaction with proteins.[39] These investigators performed μs-scale conventional MD simulations of a 14-residue peptide fragment encompassing the B1 peptide in the presence of their model of Ag^+. Interestingly, they observe a marginal increase in peptide helicity, suggesting that a nonbonded approach might be suited to simulate silver-induced folding. However, they do not comment on the structural mechanism involved, nor do they evaluate the helix propensity by quantitative simulation methods. Therefore, their study indicates that nonbonded models might constitute a valuable direction for the computational investigation of the structural consequences of silver binding to proteins, to be pursued alongside the bonded approach. Overall, together with complementary recent reports,[27,39] our study contributes to understanding silver−protein interactions and sets the stage for computational investigations of the bacterial silver-resistance machinery.

■ ASSOCIATED CONTENT

Supporting Information

The Supporting Information is available free of charge at https://pubs.acs.org/doi/10.1021/acs.jpclett.6c00044.

Details of the modelling procedure, temperature replica-exchange molecular dynamics simulations, mapping the conformational space of B1 with an Autoencoder neural network, String method analysis of B1's folding pathways, NMR of the B1 E6Q mutant peptide, Mass Spectrometry of the wildtype B1 peptide, figures of models, trajectories, potential energies, energy landscapes, neural network data, variable comparison, RMSD; tables of force-field parameters, charge distributions, T-REMD simulations, bandwidths, autoencoder training protocol and hyperparameters, collective variables (PDF)

■ AUTHOR INFORMATION

Corresponding Authors

Florian E. C. Blanc − *Université de Lyon, CNRS, UCB Lyon1, Institut des Sciences Analytiques, UMR5280 Villeurbanne, France;* orcid.org/0000-0002-0762-0478; Email: florian.blanc@isa-lyon.fr

Olivier Walker − *Université de Lyon, CNRS, UCB Lyon1, Institut des Sciences Analytiques, UMR5280 Villeurbanne, France;* orcid.org/0000-0001-7284-2555; Email: olivier.walker@univ-lyon1.fr

Authors

Maggy Hologne − *Université de Lyon, CNRS, UCB Lyon1, Institut des Sciences Analytiques, UMR5280 Villeurbanne, France;* orcid.org/0000-0002-4977-7887

Marion Girod − *Université de Lyon, CNRS, UCB Lyon1, Institut des Sciences Analytiques, UMR5280 Villeurbanne, France;* orcid.org/0000-0003-0728-2111

Mélodie Demontrond − *Université de Lyon, CNRS, UCB Lyon1, Institut des Sciences Analytiques, UMR5280 Villeurbanne, France*

Henry Chermette − *Université de Lyon, CNRS, UCB Lyon1, Institut des Sciences Analytiques, UMR5280 Villeurbanne, France;* orcid.org/0000-0002-5890-7479

Complete contact information is available at: https://pubs.acs.org/10.1021/acs.jpclett.6c00044

Notes

The authors declare no competing financial interest.

■ ACKNOWLEDGMENTS

This project received funding from French Agence Nationale de la Recherche (ANR) Resist2Silver (grant ANR-22-CE11-00-01). This project was provided with HPC and storage resources by GENCI at CINES and IDRIS thanks to the grants AD010714601 and A0180716223 on the supercomputer Adastra's MI250x partition and on the supercomputer Jean Zay's V100 partition. We thank the support engineers at CINES and IDRIS for technical assistance.

■ REFERENCES

(1) Sharma, S. K.; Goloubinoff, P.; Christen, P. Heavy Metal Ions Are Potent Inhibitors of Protein Folding. *Biochem. Biophys. Res. Commun.* **2008**, *372*, 341−345.

(2) Leal, S. S.; Botelho, H. M.; Gomes, C. M. Metal Ions as Modulators of Protein Conformation and Misfolding in Neurodegeneration. *Coord. Chem. Rev.* **2012**, *256*, 2253−2270.

(3) Tamás, M.; Sharma, S.; Ibstedt, S.; Jacobson, T.; Christen, P. Heavy Metals and Metalloids As a Cause for Protein Misfolding and Aggregation. *Biomolecules* **2014**, *4*, 252−267.

(4) Wilson, C. J.; Apiyo, D.; Wittung-Stafshede, P. Role of Cofactors in Metalloprotein Folding. *Q. Rev. Biophys.* **2004**, *37*, 285−314.

(5) Besold, A. N.; Michel, S. L. J. Neural Zinc Finger Factor/Myelin Transcription Factor Proteins: Metal Binding, Fold, and Function. *Biochemistry* **2015**, *54*, 4443−4452.

(6) Ariöz, C.; Wittung-Stafshede, P. Folding of Copper Proteins: Role of the Metal? *Q. Rev. Biophys.* **2018**, *51*, No. e4.

(7) Chabert, V.; Hologne, M.; Sénèque, O.; Crochet, A.; Walker, O.; Fromm, K. M. Model Peptide Studies of Ag^+ Binding Sites from the Silver Resistance Protein SilE. *Chem. Commun.* **2017**, *53*, 6105−6108.

(8) Chabert, V.; Hologne, M.; Sénèque, O.; Walker, O.; Fromm, M. K. Alpha-Helical Folding of SilE Models upon Ag(His)(Met) Motif Formation. *Chem. Commun.* **2018**, *54*, 10419−10422.

(9) Monneau, Y.; Arrault, C.; Duroux, C.; Martin, M.; Chirot, F.; Mac Aleese, L.; Girod, M.; Comby-Zerbino, C.; Hagège, A.; Walker, O.; et al. Structural and Dynamical Insights into SilE Silver Binding from Combined Analytical Probes. *Phys. Chem. Chem. Phys.* **2023**, *25*, 3061−3071.

(10) Asiani, K. R.; Williams, H.; Bird, L.; Jenner, M.; Searle, M. S.; Hobman, J. L.; Scott, D. J.; Soultanas, P. SilE Is an Intrinsically Disordered Periplasmic "Molecular Sponge" Involved in Bacterial Silver Resistance. *Mol. Microbiol.* **2016**, *101*, 731−742.

(11) Gupta, A.; Matsui, K.; Lo, J.-F.; Silver, S. Molecular Basis for Resistance to Silver Cations in Salmonella. *Nature Medicine* **1999**, *5*, 183−188.
(12) Silver, S. Bacterial Silver Resistance: Molecular Biology and Uses and Misuses of Silver Compounds. *FEMS Microbiology Reviews* **2003**, *27*, 341−353.
(13) McNeilly, O.; Mann, R.; Hamidian, M.; Gunawan, C. Emerging Concern for Silver Nanoparticle Resistance in Acinetobacter Baumannii and Other Bacteria. *Frontiers in Microbiology* **2021**, *12*, 894.
(14) Medici, S.; Peana, M.; Nurchi, V. M.; Zoroddu, M. A. Medical Uses of Silver: History, Myths, and Scientific Evidence. *J. Med. Chem.* **2019**, *62*, 5923−5943.
(15) Morones-Ramirez, J. R.; Winkler, J. A.; Spina, C. S.; Collins, J. J. Silver Enhances Antibiotic Activity Against Gram-Negative Bacteria. *Science Translational Medicine* **2013**, *5*, 190ra81.
(16) Wang, H.; Wang, M.; Xu, X.; Gao, P.; Xu, Z.; Zhang, Q.; Li, H.; Yan, A.; Kao, R. Y.-T.; Sun, H. Multi-Target Mode of Action of Silver against Staphylococcus Aureus Endows It with Capability to Combat Antibiotic Resistance. *Nat. Commun.* **2021**, *12*, 3331.
(17) Frei, A.; Verderosa, A. D.; Elliott, A. G.; Zuegg, J.; Blaskovich, M. A. T. Metals to Combat Antimicrobial Resistance. *Nature Reviews Chemistry* **2023**, *7*, 202−224.
(18) Zingale, G. A.; Oliveri, V.; Grasso, G. Insights into the Binding of Ag Ions with SilE Model Peptides: An NMR and MS Coupled Approach. *Metallomics* **2023**, *15*, mfad015.
(19) Bianchi, A.; Marquenet, F.; Manciocchi, L.; Spichty, M.; Fromm, K. M. Toward Predicting Silver Ion Binding in Proteins. *Chem. Commun.* **2025**, *61*, 5309.
(20) Babel, L.; Nguyen, M.-H.; Mittelheisser, C.; Martin, M.; Fromm, K. M.; Walker, O.; Hologne, M. NMR Reveals the Interplay between SilE and SilB Model Peptides in the Context of Silver Resistance. *Chem. Commun.* **2021**, *57*, 8726−8729.
(21) Arrault, C.; Monneau, Y. R.; Martin, M.; Cantrelle, F.-X.; Boll, E.; Chirot, F.; Comby Zerbino, C.; Walker, O.; Hologne, M. The Battle for Silver Binding: How the Interplay between the SilE, SilF and SilB Proteins Contributes to the Silver Efflux Pump Mechanism. *J. Biol. Chem.* **2023**, *299*, 105004.
(22) Huang, J.; Rauscher, S.; Nawrocki, G.; Ran, T.; Feig, M.; de Groot, B. L.; Grubmüller, H.; MacKerell, A. D., Jr CHARMM36m: An Improved Force Field for Folded and Intrinsically Disordered Proteins. *Nat. Methods* **2017**, *14*, 71−73.
(23) Robustelli, P.; Piana, S.; Shaw, D. E. Developing a Molecular Dynamics Force Field for Both Folded and Disordered Protein States. *Proc. Natl. Acad. Sci. U. S. A.* **2018**, *115*, E4758−E4766.
(24) Li, P.; Merz, K. M. Metal Ion Modeling Using Classical Mechanics. *Chem. Rev.* **2017**, *117*, 1564−1686.
(25) Vidossich, P.; Magistrato, A. QM/MM Molecular Dynamics Studies of Metal Binding Proteins. *Biomolecules* **2014**, *4*, 616−645.
(26) Chakravorty, D. K.; Wang, B.; Ucisik, M. N.; Merz, K. M. Insight into the Cation-π Interaction at the Metal Binding Site of the Copper Metallochaperone CusF. *J. Am. Chem. Soc.* **2011**, *133*, 19330−19333.
(27) Lithgo, R. M.; Hanževački, M.; Harris, G.; Kamps, J. J.; Holden, E.; Gianga, T.-M.; Benesch, J. L.; Jäger, C. M.; Croft, A. K.; Hussain, R.; et al. The Adaptability of the Ion-Binding Site by the Ag(I)/Cu(I) Periplasmic Chaperone SilF. *J. Biol. Chem.* **2023**, *299*, 105331.
(28) Hazel, A. J.; Walters, E. T.; Rowley, C. N.; Gumbart, J. C. Folding Free Energy Landscapes of β -Sheets with Non-Polarizable and Polarizable CHARMM Force Fields. *J. Chem. Phys.* **2018**, *149*, 072317.
(29) Leontyev, I. V.; Stuchebrukhov, A. A. Electronic Continuum Model for Molecular Dynamics Simulations. *J. Chem. Phys.* **2009**, *130*, 085102.
(30) Leontyev, I. V.; Stuchebrukhov, A. A. Electronic Continuum Model for Molecular Dynamics Simulations of Biological Molecules. *J. Chem. Theory Comput.* **2010**, *6*, 1498−1508.
(31) Du, S.; Fu, H.; Shao, X.; Chipot, C.; Cai, W. Addressing Polarization Phenomena in Molecular Machines Containing Transition Metal Ions with an Additive Force Field. *J. Chem. Theory Comput.* **2019**, *15*, 1841−1847.
(32) Li, P.; Roberts, B. P.; Chakravorty, D. K.; Merz, K. M. Rational Design of Particle Mesh Ewald Compatible Lennard-Jones Parameters for + 2 Metal Cations in Explicit Solvent. *J. Chem. Theory Comput.* **2013**, *9*, 2733−2748.
(33) Li, P.; Song, L. F.; Merz, K. M. J. Systematic Parameterization of Monovalent Ions Employing the Nonbonded Model. *J. Chem. Theory Comput.* **2015**, *11*, 1645−1657.
(34) Song, L. F.; Sengupta, A.; Merz, K. M. Thermodynamics of Transition Metal Ion Binding to Proteins. *J. Am. Chem. Soc.* **2020**, *142*, 6365−6374.
(35) Li, Z.; Song, L. F.; Sharma, G.; Koca Fındık, B.; Merz, K. M. J. Accurate Metal−Imidazole Interactions. *J. Chem. Theory Comput.* **2023**, *19*, 619−625.
(36) Li, Z.; Bhowmik, S.; Sagresti, L.; Brancato, G.; Smith, M.; Benson, D. E.; Li, P.; Merz, K. M. Simulating Metal-Imidazole Complexes. *J. Chem. Theory Comput.* **2024**, *20*, 6706−6716.
(37) Li, P.; Merz, K. M. J. Taking into Account the Ion-Induced Dipole Interaction in the Nonbonded Model of Ions. *J. Chem. Theory Comput.* **2014**, *10*, 289−297.
(38) Li, P.; Song, L. F.; Merz, K. M. J. Parameterization of Highly Charged Metal Ions Using the 12−6-4 LJ-Type Nonbonded Model in Explicit Water. *J. Phys. Chem. B* **2015**, *119*, 883−895.
(39) Manciocchi, L.; Bianchi, A.; Mazan, V.; Potapov, M.; Fromm, K. M.; Spichty, M. Modeling the Interaction Between Silver(I) Ion and Proteins with 12−6 Lennard-Jones Potential: A Bottom-Up Parameterization Approach. *Biophysica* **2025**, *5*, 7.
(40) Chen, X.; Karpenko, A.; Lopez-Acevedo, O. Silver-Mediated Double Helix: Structural Parameters for a Robust DNA Building Block. *ACS Omega* **2017**, *2*, 7343−7348.
(41) Maragliano, L.; Fischer, A.; Vanden-Eijnden, E.; Ciccotti, G. String Method in Collective Variables: Minimum Free Energy Paths and Isocommittor Surfaces. *J. Chem. Phys.* **2006**, *125*, 024106.
(42) Seminario, J. M. Calculation of Intramolecular Force Fields from Second-Derivative Tensors. *Int. J. Quantum Chem.* **1996**, *60*, 1271−1277.
(43) Talmazan, R.; Podewitz, M. PyConSolv: A Python Package for Conformer Generation of (Metal-Containing) Systems in Explicit Solvent. *J. Chem. Inf. Model.* **2023**, *63*, 5400.
(44) Perdew, J. P.; Burke, K.; Ernzerhof, M. Generalized Gradient Approximation Made Simple. *PHYSICAL REVIEW LETTERS* **1996**, *77*, 3865.
(45) Adamo, C.; Barone, V. Toward Reliable Density Functional Methods without Adjustable Parameters: The PBE0Model. *J. Chem. Phys.* **1999**, *110*, 6158−6170.
(46) Weigend, F.; Ahlrichs, R. Balanced Basis Sets of Split Valence, Triple Zeta Valence and Quadruple Zeta Valence Quality for H to Rn: Design and Assessment of Accuracy. *Phys. Chem. Chem. Phys.* **2005**, *7*, 3297.
(47) Andrae, D.; Häussermann, U.; Dolg, M.; Stoll, H.; Preuss, H. Energy-Adjusted ab Initio Pseudopotentials for the Second and Third Row Transition Elements. *Theoretica Chimica Acta* **1990**, *77*, 123−141.
(48) Bayly, C. I.; Cieplak, P.; Cornell, W.; Kollman, P. A. A Well-Behaved Electrostatic Potential Based Method Using Charge Restraints for Deriving Atomic Charges: The RESP Model. *J. Phys. Chem.* **1993**, *97*, 10269−10280.
(49) Pavlova, A.; Parks, J. M.; Gumbart, J. C. Development of CHARMM-Compatible Force-Field Parameters for Cobalamin and Related Cofactors from Quantum Mechanical Calculations. *J. Chem. Theory Comput.* **2018**, *14*, 784−798.
(50) Schauperl, M.; Nerenberg, P. S.; Jang, H.; Wang, L.-P.; Bayly, C. I.; Mobley, D. L.; Gilson, M. K. Non-Bonded Force Field Model with Advanced Restrained Electrostatic Potential Charges (RESP2). *Communications Chemistry* **2020**, *3*, 44.
(51) Durell, S. R.; Brooks, B. R.; Ben-Naim, A. Solvent-Induced Forces between Two Hydrophilic Groups. *J. Phys. Chem.* **1994**, *98*, 2198−2202.

https://doi.org/10.1021/acs.jpclett.6c00044
J. Phys. Chem. Lett. XXXX, XXX, XXX−XXX

(52) Sugita, Y.; Okamoto, Y. Replica-Exchange Molecular Dynamics Method for Protein Folding. *Chem. Phys. Lett.* **1999**, *314*, 141−151.
(53) Okabe, T.; Kawata, M.; Okamoto, Y.; Mikami, M. Replica-Exchange Monte Carlo Method for the Isobaric−Isothermal Ensemble. *Chem. Phys. Lett.* **2001**, *335*, 435−439.
(54) Patriksson, A.; van der Spoel, D. A Temperature Predictor for Parallel Tempering Simulations. *Phys. Chem. Chem. Phys.* **2008**, *10*, 2073−2077.
(55) Fiorin, G.; Klein, M. L.; Hénin, J. Using Collective Variables to Drive Molecular Dynamics Simulations. *Mol. Phys.* **2013**, *111*, 3345−3362.
(56) Shirts, M. R.; Chodera, J. D. Statistically Optimal Analysis of Samples from Multiple Equilibrium States. *J. Chem. Phys.* **2008**, *129*, 124105.
(57) Shirts, M. R.; Ferguson, A. L. Statistically Optimal Continuous Free Energy Surfaces from Biased Simulations and Multistate Reweighting. *J. Chem. Theory Comput.* **2020**, *16*, 4107−4125.
(58) Ward, M. D.; Zimmerman, M. I.; Meller, A.; Chung, M.; Swamidass, S. J.; Bowman, G. R. Deep Learning the Structural Determinants of Protein Biochemical Properties by Comparing Structural Ensembles with DiffNets. *Nat. Commun.* **2021**, *12*, 3023.
(59) Lemke, T.; Peter, C. EncoderMap: Dimensionality Reduction and Generation of Molecule Conformations. *J. Chem. Theory Comput.* **2019**, *15*, 1209−1215.
(60) Lemke, T.; Berg, A.; Jain, A.; Peter, C. EncoderMap(II): Visualizing Important Molecular Motions with Improved Generation of Protein Conformations. *J. Chem. Inf. Model.* **2019**, *59*, 4550−4560.
(61) Ceriotti, M.; Tribello, G. A.; Parrinello, M. Simplifying the Representation of Complex Free-Energy Landscapes Using Sketch-Map. *Proc. Natl. Acad. Sci. U. S. A.* **2011**, *108*, 13023−13028.
(62) Tenenbaum, J. B.; de Silva, V.; Langford, J. C. A Global Geometric Framework for Nonlinear Dimensionality Reduction. *Science* **2000**, *290*, 2319−2323.
(63) Das, P.; Moll, M.; Stamati, H.; Kavraki, L. E.; Clementi, C. Low-Dimensional, Free-Energy Landscapes of Protein-Folding Reactions by Nonlinear Dimensionality Reduction. *Proc. Natl. Acad. Sci. U. S. A.* **2006**, *103*, 9885−9890.
(64) E, W.; Ren, W.; Vanden-Eijnden, E. String Method for the Study of Rare Events. *Phys. Rev. B* **2002**, *66*, 052301.
(65) Pan, A. C.; Sezer, D.; Roux, B. Finding Transition Pathways Using the String Method with Swarms of Trajectories. *J. Phys. Chem. B* **2008**, *112*, 3432−3440.
(66) Moradi, M.; Enkavi, G.; Tajkhorshid, E. Atomic-Level Characterization of Transport Cycle Thermodynamics in the Glycerol-3-Phosphate:Phosphate Antiporter. *Nat. Commun.* **2015**, *6*, 8393.
(67) Blanc, F. E. C.; Houdusse, A.; Cecchini, M. A Weak Coupling Mechanism for the Early Steps of the Recovery Stroke of Myosin VI: A Free Energy Simulation and String Method Analysis. *PLOS Computational Biology* **2024**, *20*, No. e1012005.
(68) Kutchukian, P. S.; Yang, J. S.; Verdine, G. L.; Shakhnovich, E. I. All-Atom Model for Stabilization of α-Helical Structure in Peptides by Hydrocarbon Staples. *J. Am. Chem. Soc.* **2009**, *131*, 4622−4627.
(69) Smith, S. J.; Du, K.; Radford, R. J.; Tezcan, F. A. Functional, Metal-Based Crosslinkers for α-Helix Induction in Short Peptides. *Chemical Science* **2013**, *4*, 3740.
(70) Smith, S. J.; Radford, R. J.; Subramanian, R. H.; Barnett, B. B.; Figueroa, J. S.; Tezcan, F. A. Tunable Helicity, Stability and DNA-binding Properties of Short Peptides with Hybrid Metal Coordination Motifs. *Chemical Science* **2016**, *7*, 5453−5461.
(71) Fischer, N.; Tóth, A.; Jancsó, A.; Thulstrup, P.; Diness, F. Inducing α-Helicity in Peptides by Silver Coordination to Cysteine. *Chemistry − A European Journal* **2024**, *30*, No. e202304064.
(72) Richardson-Matthews, R.; Velko, K.; Bhunia, B.; Ghosh, S.; Oktawiec, J.; Brunzelle, J. S.; Dang, V. T.; Nguyen, A. I. Metal-α-Helix Peptide Frameworks. *J. Am. Chem. Soc.* **2025**, *147*, 17433−17447.
(73) Monticelli, L.; Tieleman, D. P.; Colombo, G. Mechanism of Helix Nucleation and Propagation: Microscopic View from Micro-second Time Scale MD Simulations. *J. Phys. Chem. B* **2005**, *109*, 20064−20067.
(74) Acharyya, A.; Ge, Y.; Wu, H.; DeGrado, W. F.; Voelz, V. A.; Gai, F. Exposing the Nucleation Site in α-Helix Folding: A Joint Experimental and Simulation Study. *J. Phys. Chem. B* **2019**, *123*, 1797−1807.
(75) Lin, M. M.; Shorokhov, D.; Zewail, A. H. Dominance of Misfolded Intermediates in the Dynamics of α-Helix Folding. *Proc. Natl. Acad. Sci. U. S. A.* **2014**, *111*, 14424−14429.

https://doi.org/10.1021/acs.jpclett.6c00044
J. Phys. Chem. Lett. XXXX, XXX, XXX−XXX